HHS Public Access

Author manuscript

Magn Reson Med. Author manuscript; available in PMC 2023 October 01.

Published in final edited form as:

Magn Reson Med. 2022 October ; 88(4): 1659–1672. doi:10.1002/mrm.29308.

OSCILLATE: A Low-Rank Approach for Accelerated Magnetic Resonance Elastography

Grace McIlvain[1], **Alex Cerjanic**[1,2], **Anthony G Christodoulou**[3], **Matthew DJ McGarry**[4], **Curtis L Johnson**[1]

[1]Department of Biomedical Engineering, University of Delaware, Newark, DE, United States

[2]University of Illinois College of Medicine, Urbana, IL, United States

[3]Biomedical Imaging Research Institute, Cedars-Sinai Medical Center, Los Angeles, CA, United States

[4]Thayer School of Engineering, Dartmouth College, Hanover, NH, United States

Abstract

Purpose: Magnetic resonance elastography (MRE) is a technique to characterize brain mechanical properties *in vivo*. Due to the need to capture tissue deformation in multiple directions over time, MRE is an inherently long acquisition, which limits achievable resolution and use in challenging populations. The purpose of this work is to develop a method for accelerating MRE acquisition by using low-rank image reconstruction to exploit inherent spatiotemporal correlations in MRE data.

Methods: The proposed MRE sampling and reconstruction method, OSCILLATE, involves alternating which *k*-space points are sampled between each repetition by a reduction factor, $R_{OSC.}$ Using a predetermined temporal basis from a low-resolution navigator in a joint low-rank image reconstruction, all images can be accurately reconstructed from a reduced amount of *k*-space data.

Results: Decomposition of MRE displacement data demonstrated that, on average, 96.1% of all energy from an MRE dataset is captured at rank $L = 12$ (reduced from a full rank of 24). Retrospectively undersampling data with $R_{OSC} = 2$ and reconstructing at low-rank ($L = 12$) yields highly accurate stiffness maps with voxel-wise error of 5.8% ± 0.7%. Prospectively undersampled data at $R_{OSC} = 2$ were successfully reconstructed without loss of material property map fidelity, with average global stiffness error of 1.0% ± 0.7% compared to fully-sampled data.

Conclusions: OSCILLATE produces whole-brain MRE data at 2 mm isotropic resolution in 1 minute 48 sec.

Keywords

Elastography; Viscoelasticity; Low-Rank; Joint Image Reconstruction; Brain

Corresponding Author: Curtis L Johnson, PhD, 150 Academy St, Newark, DE 19716, clj@udel.edu.

INTRODUCTION

Microstructural integrity of neural tissue can be assessed through its mechanical properties using magnetic resonance elastography (MRE)[1]. MRE has had growing interest as a neuroimaging technique for its ability to sensitively analyze brain development[2,3], degeneration[4–6], and cognitive function[7,8]. MRE measures properties such as viscoelasticity, poroelasticity, and material anisotropy *in vivo* through phase contrast-based MRI. To accurately capture full vector tissue deformation in time, it is necessary to collect repeated acquisitions with different motion encodings, making MRE a fundamentally long scan. This requirement for repeated measurements has imposed limits on several aspects of MRE research, such as use on populations who have trouble laying still for extended periods of time including children[9]. Further, the long acquisition times limit achievable spatial resolution necessary to study small anatomical areas, such as the subfields of the hippocampus[10] and thin sections of the cerebral cortex[11]. And recent techniques involving multiple MRE datasets, such as multiple actuations to study brain anisotropic properties[12–15] or multiple frequencies to study brain frequency-dependent material properties[16,17], are limited in number of scans possible or useable spatial resolution in order to keep exams at reasonable length.

Previous research aimed at improving MRE sequence speeds have sought to reduce the time it takes to sample one image, including through parallel imaging[18], compressed sensing[19], use of 3D non-Cartesian *k*-space sampling[20–22], and acquisition at higher field strength[23]. Other techniques have focused on acceleration through manipulating how the MRE displacements are sampled, including the use of simultaneously applied motion encoding gradients (MEGs)[24–27] or use of multiple interleaved encoding directions, such as in eXpresso-MRE[28] and ristretto-MRE[29]. While these approaches are well-developed and can be applied to many MRE problems, they often require lower maximum gradient strengths that result in reduced signal-to-noise ratio (SNR). Further advancements in acquisition speeds would allow high-resolution MRE to be more readily adopted for clinical use.

Here we propose to accelerate MRE acquisitions by exploiting spatiotemporal redundancy in the data through sparse sampling and low-rank joint image reconstruction. Low-rank methods work by estimating a low-dimensional temporal subspace from auxiliary data and enforcing this subspace during image reconstruction[30,31]. Ideally, these subspaces are able to accurately describe the entire image signal if the data is highly correlated[32]. Model based low-rank image reconstructions for time series data have been successfully applied in many applications for data which is fundamentally spatiotemporally redundant. In MRI, time series low-rank models have been used for accelerating acquisitions including spectroscopic imaging[33], T_2 mapping[34], diffusion[35], fMRI[36–38], and cardiac imaging[39–41]. An MRE dataset comprises multiple highly spatiotemporally correlated time-resolved phase encodings of harmonic motion in different directions. Thus, we propose that MRE data can be modeled and reconstructed at a reduced rank by leveraging these inherent spatiotemporal correlations.

In this work we introduce OSCILLATE (Observing Spatiotemporal Correlations for Imaging with Low-rank Leveraged Acceleration in Turbo Elastography)[42], a method of accelerating MRE acquisition with negligible loss in data fidelity via sparse sampling and low-rank image reconstruction. The proposed method allows for acceleration of multishot MRE acquisitions capable of achieving high spatial resolution. Here we describe the theory behind low-rank image reconstructions and demonstrate the feasibility of modeling brain MRE data at a reduced rank. We demonstrate the accuracy of retrospectively and prospectively under sampling MRE data from a spin-echo multiband, multishot spiral MRE sequence and reconstructing it with OSCILLATE.

THEORY

MRE Image Theory

MRE measures displacements of viscoelastic tissue induced via harmonic mechanical vibration, encoded to the phase of the images through motion encoding gradients (MEGs). The different time points are achieved by phase offsets where the onset of mechanical vibration relative to the MEGs is varied. The resulting phase of the MRE signal, $\phi(r, n)$, can be generally described as a function of space and time. The spatial distribution of phase is given by $\phi_0(r)$ which is modulated in time harmonically with a spatially-varying phase relative to the applied vibration of $\varphi(r)$. Images are sampled with N phase offsets evenly spaced over one period of vibration, such that the phase of any sample in time, n, is given by:

$$\phi(r,n) = \phi_0(r)\ \sin\left(2\pi\frac{n}{N} + \varphi(r)\right). \quad (1)$$

This phase gets mapped on a common complex image, $\rho_0(r)$, such that a complete MRE dataset is a series of complex images, $\rho(r, n)$:

$$\rho(r,n) = \rho_0(r)e^{-i\phi_0(r)\sin\left(2\pi\frac{n}{N} + \varphi(r)\right)}. \quad (2)$$

In addition to N phase offsets, a complete MRE dataset consists of images with both positive and negative MEG polarity, which are subtracted during post-processing to amplify contrast and remove static background phase. Additionally, MEGs are applied separately along the phase, read, and slice directions, which allow full vector displacement fields to be recovered. Therefore, the entire acquisition consists of a set of repetitions (phase offsets × polarities × MEG directions) that are identical in magnitude and with varying phase. Here we propose to express this MRE data as a pseudo-time series, τ, consisting of all repetitions, where τ indexes the acquired combinations of phase offset × direction × gradient polarity, and the final image series which we seek to recover is $\rho(r, \tau)$. In k-space we can consider this as $d(k,\tau) = \mathcal{F}_r\{\rho(r,\tau)\}$. An MRE scan consisting of x number of phase offsets and y number of encodings (encompassing directions and polarities) would be considered to have a full rank of L = $x \times y$.

Low-Rank Modeling

MRE data can be considered low-rank in the sense that a reduced number of temporal basis functions and spatial coefficients can describe the entire dataset[43]. MRE data is highly correlated and can be modeled as an L-th order partially-separable function in image space:

$$\rho(r,\tau) = \sum_{\ell=1}^{L} \psi_\ell(r)\varphi_\ell(\tau), \tag{3}$$

such that its Casorati matrix, $C = \Psi\Phi$, with elements $C_{ij} = \rho(r_i, \tau_j)$ has rank $L \leq 24$, where $\Psi_{ij} = \psi_j(r_i)$ are spatial coefficient maps and $\Phi_{ij} = \varphi_i(\tau_j)$ are temporal basis functions. Here the data is reshaped into a Casorati matrix of rows comprising all discretized spatial locations versus a 'time' dimension comprising all repetitions (i.e. directions, phase offsets, and gradient polarities). This relationship can be written in k-space as:

$$d(k,\tau) = \sum_{\ell=1}^{L} \tilde{\psi}_\ell(k)\varphi_\ell(\tau); \quad \text{where } \tilde{\psi}_\ell = \mathcal{F}\{\psi_\ell(r)\}. \tag{4}$$

To estimate the Φ for a system, a singular value decomposition (SVD) can be performed on the Casorati matrix, $C(r) = U\Sigma V^H$, where V^H is the set of temporal basis functions and Σ is the singular value matrix. Σ and V^H are sorted in descending order of significance, with the highest order singular values corresponding to the basis function which contributes the most energy to the signal, and all subsequent singular values corresponding to the relative contributions of the remaining basis functions. Sorted in this order, and with $V^H = \Phi$, we can truncate the rank of C to L, thereby retaining only the bases contributing the most energy to the signal. The remaining energy and bases primarily consists of random noise and information with less well-defined spatiotemporal coherence, such as would arise from spurious vibrations and physiological motions present in brain MRE data[44], and thus does not add additional useful information to the MRE displacement image reconstruction. Ultimately, by reconstructing information at a low-dimensional temporal subspace, less k-space sampling is necessary to recover the entire set of images.

Low-Rank Reconstruction

We can take advantage of the low-rank nature of MRE data in a joint reconstruction framework. If we have an estimate of the temporal basis Φ, a matrix of spatial coefficients, Ψ, can be iteratively solved for through the objective function:

$$\hat{\Psi} = \text{argmin}_{\Psi} \| d(k,\tau) - E\{\Psi\Phi\} \|_2^2 + \beta\mathcal{R}\{\Psi\Phi\}, \tag{5}$$

where $d(k, \tau)$ is the acquired k-space data, E is the sampling operator, and $\mathcal{R}$ is a regularization penalty with scaling factor β. The sequence chosen to implement low-rank undersampling and reconstruction must consist of multiple readouts per volume and must allow for predetermination of the temporal basis, Φ. The encoding operator, E, encompasses all sampled k-space locations and their distribution across repetitions, and thus also how data is undersampled. The undersampling pattern in k-space is permitted to be distributed across temporal points to take advantage of joint reconstruction. A depiction of the OSCILLATE reconstruction method can be seen in Figure 1.

METHODS

OSCILLATE Implementation

3D Multiband, Multishot Spiral MRE Sequence—The proposed OSCILLATE acquisition was built from a foundation of a 3D multiband, multishot spiral, spin-echo MRE sequence[45] (Figure 2). This sequence uses a multiband RF pulse to excite several evenly distributed slices that together form a 3D volume, which is encoded in *k*-space with a stack of 2D constant density interleaved spirals[46]. Using this approach, SENSE parallel imaging[47] can be applied in-plane by undersampling k_{xy}-shots and thru-plane by undersampling k_z-planes, for a total reduction factor of $R_{SENSE} = R_{xy} \times R_z$. This sequence uses a low-resolution 3D navigator image (matrix 40 × 40 × 4), sampled once per spiral readout, to capture any motion-induced phase error between excitations that can be compensated for during image reconstruction[48]. The navigator is sampled using a spiral-in trajectory blipped between k_z-planes[49]. These navigator images have the same phase and image contrast as the MRE image data to which they belong, and thus also the same temporal basis. Nonlinear motion-induced phase error correction is achieved via the phase corrected SENSE algorithm, which applies the conjugate of the navigator phase to each associated shot during image reconstruction via the use of a shot specific SENSE map incorporating the conjugate of the error measured by the navigator phase[50], which reduces shot-to-shot variation in phase arising from spurious vibrations and physiological motions[44]. Data is reconstructed accounting for B_0 field inhomogeneities via a fieldmap collected immediately prior to MRE data collection[51,52]. Images are reconstructed iteratively using a preconditioned conjugate gradient solver implementing non-Cartesian SENSE[47] with field inhomogeneity correction via time segmentation with one time segment per 2.8 ms of readout length, using the non-uniform fast Fourier transform (NUFFT)[51]. Regularization is achieved through a first order quadratic roughness penalty applied only to the in-plane direction with no penalization through-plane or across repetitions. Reconstructions are performed using PowerGrid[53], which leverages graphical processing units (GPUs) to enable faster image reconstruction.

OSCILLATE Sampling—The OSCILLATE sampling scheme undersamples multishot data in a distributed fashion across repetitions, with reduction factor indicated by R_{OSC}. The implemented scheme is built on the multiband sequence designed for 2 mm resolution, which includes 4 interleaved constant density spiral k_{xy}-shots[46], each shot having a readout time of 13.89 ms, in 4 k_z-planes from a multiband excitation of 4 slices evenly distributed across the imaging volume (of 64 total slices). In this case we are applying R_{OSC} in addition to SENSE parallel imaging with $R_{xy} = 2$ and $R_z = 2$ for a total $R_{SENSE} = 4$. Here we explore different OSCILLATE sampling schemes. To achieve $R_{OSC} = 2$ we can either alternate which k_{xy}-shots were sampled between each repetition, resulting in one sampled shot in each of the two planes, or we can alternate which k_z-plane were sampled for each repetition, for two shots in just one plane. These $R_{OSC} = 2$ undersampling options are in addition to the four-fold reduction from paralleling imaging, resulting in an eight-fold under sampling from the fully-sampled sequence ($R_{TOTAL} = R_{SENSE} \times R_{OSC}$). We also explore $R_{OSC} = 4$ by simultaneously undersampling both k_{xy}-shots and k_z-planes.

OSCILLATE Reconstruction—The OSCILLATE low-rank image reconstruction uses the same algorithm as the multiband MRE images as described above and includes SENSE parallel imaging[47], B_0 field inhomogeneity correction[51], and nonlinear motion-induced phase error correction[50]. However, in the OSCILLATE reconstruction, we predetermine the temporal basis function Φ from the low-resolution, phase-corrected navigator images, which are collected once per readout and are reconstructed prior to the full-resolution image reconstruction. A singular value decomposition (SVD) is performed on the reconstructed phase-corrected navigator images to determine Φ, which is then used to solve for spatial coefficients Ψ during reconstruction according to Eq. 5. The OSCILLATE reconstruction is a joint reconstruction in that data from all 24 repetitions are used simultaneously to solve for the shared spatial coefficients.

Data Collection

Five healthy adult subjects (2 male / 3 female; age 21–27 years) completed an imaging session on a Siemens 3T Prisma MRI scanner (Siemens Medical Solutions; Erlangen, Germany) with a 64-channel RF-receive coil. This study was approved by the University of Delaware Institutional Review Board and all subjects provided informed written consent. The scanning session included a fieldmap scan and two MRE scans, which included a typical multiband MRE scan ($R_{SENSE} = 4$) and a prospectively undersampled OSCILLATE scan with additional $R_{OSC} = 2$ ($R_{TOTAL} = 8$). Each scan had imaging parameters that included: 240 × 240 mm^2 FOV; 120 × 120 matrix; 64 slices; TR/TE = 2240/70 ms; 2.0 × 2.0 × 2.0 mm^3 resolution; bilateral, flow-compensated, matched-period motion-encoding gradients at 70 mT/m; and 4 evenly-spaced phase offsets. The multiband MRE acquisition time was 3 minutes 15 seconds. The OSCILLATE scan had prospectively undersampled shots, where an alternating pattern of which k_{xy} shot was acquired for each of the 24 repetitions for a resulting reduction factor of $R_{OSC} = 2$; all other scan parameters remained the same. The OSCILLATE scan took 1 minute 48 seconds. For both scans, displacements from 50 Hz vibrations were delivered to the head via a pneumatic actuator system with passive pillow driver (Resoundant, Inc.; Rochester, MN). Each of the MRE scans included a separately collected fieldmap scan with parameters including: 240 × 240 mm^2 FOV; 120 × 120 matrix; 64 slices; and TR/TE_1/TE_2 = 3200/15.0/15.9 ms. The scanning session also included a high resolution T_1-weighted MPRAGE (magnetization-prepared rapidly-acquired gradient echo) scan for anatomical segmentation (0.9 × 0.9 × 0.9 mm^3 voxel size; TR/TI/TE = 1900/900/2.32 ms).

Experiment 1: Low-Rank Truncation

We examined the effective rank of MRE data by decomposing the reconstructed multiband MRE data using SVD. Image data was then truncated to a series of reduced rank matrices according to the SVD by retaining only data in ranks 1 through L, with L equal to 24 (full-rank), 21, 18, 15, 12, and 9. Each truncated image was processed into maps of shear stiffness using the nonlinear inversion algorithm (NLI), which converts MRE displacement data into estimates of brain tissue viscoelastic properties[54,55]. NLI returns the complex shear modulus of the tissue ($G = G' + iG''$), which comprises the storage (G') and loss (G'') moduli, and from which the shear stiffness is calculated as $\mu = 2|G|^2/(G' + |G|)^1$. The normalized

root-mean-squared error (NRMSE) was calculated between stiffness maps from each of the truncated datasets ($\mu_{L<24}$) and the corresponding full rank dataset ($\mu_{L=24}$) according to:

$$NRMSE = \frac{\|\mu_{L=24} - \mu_{L<24}\|_F}{\|\mu_{L=24}\|_F}. \quad (6)$$

In this experiment we also aimed to compare efficacy of different arrangements of the MRE data in the Casorati matrix prior to decomposition. To examine this question, we decomposed MRE data sets according to each of the following conditions: 1) the temporal component including all repetitions (in the order of gradient polarities, directions, and phase offsets), with the full MRE rank being $L = 24$; 2) gradient encoding directions included as 'space', such that the temporal dimension only includes polarities and phase offsets, with the full MRE rank being $L = 8$; and 3) treating each direction separately, such that each have their own temporal basis function, with the full MRE rank being $L = 8$. For comparison of results between conditions, the cases two and three are described as having an effective rank of L times three.

Experiment 2: Retrospective Undersampling

To demonstrate the viability of the OSCILLATE technique, we retrospectively undersampled the *k*-space data from the collected multiband MRE data for all subjects. Figure 3A shows the fully sampled *k*-space trajectory from the multiband MRE sequence while Figure 3B depicts typical undersampling reconstructed with SENSE parallel imaging (i.e. $R_{SENSE} = 4$). We tested different OSCILLATE undersampling patterns to determine performance in comparison with the original dataset. We choose two $R_{OSC} = 2$ undersampling patterns including alternating which k_{xy}-shots were sampled for each temporal repetition (Figure 3C) or alternating which k_z-plane were sampled (Figure 3D). We also tested a $R_{OSC} = 4$ reduction by undersampling both k_{xy}-shots and k_z-planes. We used this reduced amount of *k*-space data to reconstruct full image datasets in our joint low-rank reconstruction, from which stiffness maps are estimated with NLI. The image regularization used was an in-plane, first order quadratic roughness penalty with weighting β. The penalty weighting was scaled by the square of the number of shots used to maintain balance with the data consistency term in the objective function – i.e. for $R_{OSC} = 1$, $\beta = 1000$; for $R_{OSC} = 2$, $\beta = 250$; for $R_{OSC} = 4$, $\beta = 62.5$.

We determined error for each case by calculating NRMSE, as described above, and average global error between the original multiband MRE dataset ($\mu_{Rosc=1}$) and the undersampled ($\mu_{Rosc>1}$) stiffness maps as $(\mu_{Rosc=1} - \mu_{Rosc>1})/\mu_{Rosc=1}$. Finally, to demonstrate the appropriateness of using the navigator images to determine the temporal basis functions, we conducted an additional experiment in which we calculated the temporal basis from the reference multiband MRE image data ($R_{OSC} = 1$) and used the resulting Φ in the low-rank OSCILLATE reconstruction. We compared errors from reconstructions using Φ estimated from the image data and the navigator data.

Experiment 3: Prospective Undersampling

Lastly, the prospectively undersampled *k*-space data was reconstructed with OSCILLATE for comparison with multiband MRE data. The undersampling pattern used for all prospective sampling was $R_{OSC} = 2$ with alternating k_{xy}-shots sampled. Reconstructed data for all subjects was converted into maps of shear stiffness through NLI. Masks of cerebrospinal fluid (CSF) were created from the MPRAGE scan using FAST[56] and were registered to MRE data through FLIRT[57], both of which are utilities in the FMRIB Software Library (FSL)[58]. The voxels containing greater than 1% CSF were eliminated from analysis, as CSF is a fluid which does not fit the viscoelastic model. Global average stiffness error was then calculated between the multiband MRE stiffness maps and the prospectively undersampled $R_{OSC} = 2$ OSCILLATE data.

RESULTS

Experiment 1: Low-Rank Truncation

To demonstrate the low-rank nature of MRE data, we decomposed the complete MRE dataset using SVD. Figure 4 shows the normalized singular values of the five MRE datasets and the images show an example of the data described by each spatial coefficient (see Supplemental Figure S1 for magnitude and phase components of each individual spatial coefficient). Nearly all MRE data energy is captured at or below rank $L = 12$, with the sum of the singular values in basis functions 1–12 being 96.1% on average (range 94.4% to 97.2%). Data in the first temporal base represents the mean of the complex data across all repetitions, which contains the majority of the magnitude information, as this does not change between repetitions. Spatial coefficients corresponding to subsequent temporal bases depict variable patterns in the signal which occur in the time series, including the differences in phase between repetitions. We find that past the 12th base, all successive bases comprise primarily noise which does not contain meaningful signal.

Figure 5 shows the results of truncating the complex MRE data and inverting the displacement fields from reduced rank images into maps of stiffness. To determine the most accurate decomposition to describe the MRE data, we compared the performance of the MEG directions each having their own time series and all having the same time series. We found that modeling the MEG directions as spatial or temporal components of the Casorati matrix resulted in no meaningful differences to the resulting property maps, with a Wilcoxon Signed Rank test results of $p = 0.813$ (Figure 5). We opted to use the MEG directions as part of the ‘time’ dimension to provide more versatility in potential undersampling patterns. In doing so we found that MRE data is accurately described by just the first 12 bases. Reducing the rank to 21 results in a stiffness map with NRMSE of 1.6% ± 0.1% compared to full rank of 24. Further reducing the rank showed only very small increases in NRMSE to resulting mechanical property maps. Reducing the rank to $L = 12$ results in NRMSE of 2.3% ± 1.2% across subjects, which equates to a global average error of just 0.3%. We found that truncating to a rank $L < 12$ returns substantial errors in stiffness maps; for example, rank $L = 9$ has an average NRMSE of 34.6% ± 14.7%.

Experiment 2: Retrospective Undersampling

Figure 6 shows the results of retrospectively undersampling the *k*-space data acquired with the multiband MRE sequence and reconstructed with OSCILLATE with reduced rank of L = 12. Reconstruction with reduced rank but without undersampling (R_{OSC} = 1) resulted in an NRMSE of 5.2% ± 0.5%. Undersampling at R_{OSC} = 2 by alternating k_{xy}-shots resulted in an NRMSE of 5.8% ± 0.7% and global stiffness error of just 0.2% ± 0.2%. Undersampling at R_{OSC} = 2 by alternating k_z-planes resulted in NRMSE of 9.8% ± 1.5% and global stiffness error of 2.3% ± 0.6%. Undersampling both k_{xy}-shots and k_z-planes simultaneously, for an R_{OSC} = 4, resulted in an NRMSE of 13.0% ± 2.2%. We determined that undersampling k_{xy}-shots at R_{OSC} = 2 resulted in the lowest error and was used as the undersampling scheme for all other experiments. Comparing the stiffness maps which were reconstructed with temporal basis estimated from Φ from the navigator images ($\Phi_{navigator}$) and from the reference multiband MRE image series (Φ_{image}), we found high agreement between the two reconstructions. Each had approximately the same error compared to the reference stiffness map (5.1% and 5.3% NRMSE for Φ_{image} and $\Phi_{navigator}$, respectively), and with a small NRMSE of 3.5% between them, which is below the degree of variability expected from the OSCILLATE undersampling (See Supplemental Figure S2). This confirms that the navigator data is sufficient to estimate temporal basis functions describing the image series.

Figure 7 shows the R_{OSC} = 2 retrospectively undersampled stiffness maps from each of the five subjects, in comparison with the original multiband MRE reference stiffness map and the absolute error between the two scans. The average NRMSE of the OSCILLATE data was 5.8% ± 0.7% across subjects, with the largest NRMSE in any subject being 6.6%. Based on the difference maps between undersampled and reference scans, error appears largely concentrated in the ventricle region, which is expected as the ventricles are fluid and are not modeled in our inversion, and thus are less stable due to model-data mismatch. Outside of the ventricle region, the error is small in magnitude and appears to be randomly distributed across the brain in all five subjects.

Experiment 3: Prospective Undersampling

Figure 8 shows the results from the prospectively undersampled OSCILLATE sequence with R_{OSC} = 2. We found that average global stiffness error across all subjects was 1.0% ± 0.7%. The maximum average global error in any single subject between the reference scan and OSCILLATE scan was 2.3%. We did not calculate NRMSE between the two sequential scans as small subject motion between scans leads to misregistration and inflated error estimates. This 2x acceleration from OSCILLATE resulted in a scan time of 1 minute 48 seconds, which was decreased from the reference scan acquisition time of 3 minutes and 15 seconds.

DISCUSSION

In this work we present OSCILLATE, a novel MRE imaging sequence and reconstruction technique for rapid data acquisition and accurate mechanical property estimation without loss of resolution. This technique leverages the spatiotemporally correlated nature of brain MRE data and formulates the MRE problem in terms of a low-rank subspace reconstruction

problem to allow for reduction in required *k*-space data. MRE data is collected as multiple acquisitions of the same anatomical image under different phase conditions which are modulated by the same induced harmonic actuation, and thus are inherently related across repetitions. Here, we demonstrated the viability of implementing these principles in the OSCILLATE technique for two-fold acceleration of MRE acquisition time and confirm that quality of the measured mechanical properties is maintained. Our implementation of OSCILLATE added to a 3D multiband, multishot spiral, spin-echo MRE sequence resulted in whole-brain MRE data acquired in less than two minutes.

MRE data is a strong candidate for low-rank modeling, however, the most appropriate method for decomposing MRE data into its spatiotemporal components must be investigated. Theoretically, each MEG direction is sampled with the same underlying harmonic phase, and therefore could be described with the same temporal bases, which would be achieved by including this dimension as part of ‘space’ in the Casorati matrix and potentially strengthening the model. But in practice, when sampled data includes noise and motion-induced phase errors, it becomes necessary to explore how enforcing directions as part of ‘time’ or ‘space’ basis affects data decomposition and subspace formation. We found that either approach produced no significant difference in resulting property maps. We ultimately determined that considering MEG directions as part of the temporal dimension, such that the full rank of the dataset is $L = 24$, would be better suited for the MRE problem as it gives more versatility in allowing for undersampling patterns that could be distributed across the repetitions. This reduces the importance on any single repetition in the joint image reconstruction, which is beneficial in the event of unexpected subject motion or physiological noise[44].

A key aspect of a low-rank reconstruction is the accurate determination of temporal basis functions, which describe how the image repetitions are related. Navigator images are a popular MRI tool used in multishot sequences to correct for motion-induced phase errors. They are traditionally acquired once per readout, are fully-sampled but low-resolution, and offer an accurate description how the signal varies from shot-to-shot and repetition-to-repetition. The navigator images of the multiband MRE sequence are ideally suited to estimating temporal bases, as they are collected immediately before image readout and are matched in phase and image contrast. Unlike using raw *k*-space data for temporal basis estimation, the navigator images can be corrected for motion-induced phase errors prior to decomposition. While we used a navigator to determine temporal bases in this application, it may be possible to estimate these bases by other means, such as from imaging data collected using a variable density spiral[59] or a blip back EPI[60].

In this work, we demonstrate the low-rank nature of MRE data and prove maintained accuracy of the resulting stiffness map. After decomposing MRE data into its spatial and temporal bases and truncating the data to a reduced number of bases, we find that a reduced rank of $L = 12$ provides a stiffness map with NRMSE of just 2.3%. Of the total signal present in an MRE dataset, only 3.9% exists in bases above $L = 12$, on average, and these higher order bases are predominantly made of noise. This reduced rank of $L = 12$ can be considered as the minimum representing the complex, full vector displacement fields estimated through MRE imaging. Spatial distributions of three motion components are

estimated, each of which are complex, describing harmonic motion through the viscoelastic medium, for a total of six motion coefficients. Because motion is mapped in the phase of the signal, and our approach works on the complex image series with real and imaginary components, the six phase bases result in twelve bases in the entire complex series for the final rank of $L = 12$, which matches what we found experimentally. MRE data can be described at a low rank of $L = 12$ regardless of resolution, frequency of actuation, or unusual geometries such as tumors. While we demonstrated the performance of OSCILLATE using a single frequency of 50 Hz, we expect the method to work for all brain MRE data collected with a single frequency of actuation with the same low rank of $L = 12$. However, for simultaneous multifrequency MRE[28,61], we expect the required subspace would be of higher rank to capture the additional spatial displacement coefficients, and thus limiting the potential for image acceleration in some cases.

In Experiment 2, we demonstrate that the proposed OSCILLATE reconstruction can accurately recover MRE images from retrospectively undersampled data. With in-plane retrospective undersampling at $R_{OSC} = 2$, reconstructed stiffness maps have an NRMSE of 5.8%. These values are slightly higher than the error seen in Experiment 1, however this is to be expected as in this analysis we are using reduced *k*-space data with likely different phase errors between shots. Other MRE sequences typically do not report voxel-wise error, making performance comparisons challenging, however, our results show less than 6% NRMSE and just 1% global average absolute error, which is still well within the repeatability range for MRE data[62,63] and is well below the threshold for detecting group differences or finding individual differences. Undersampling by alternating k_{xy}-shots resulted in less error than by alternating k_z-planes because the spiral sampling in-plane results in incoherent artifacts from any residual aliasing, while the thru-plane sampling is Cartesian and potentially more prone to slice aliasing artifacts that may impact stiffness results.

Here, we use a nonlinear inversion to reconstruct maps of stiffness, but we would expect other MRE algorithms such as common direct inversion methods[64–66] or the recently developed neural network inversions[67,68] to behave similarly in inverting displacement maps created from low-rank data. Ultimately, we found that prospectively collected OSCILLATE data with 2x undersampling resulted in approximately 1% average error across subjects, despite the expected random noise differences between sequential scans, making error from OSCILLATE comparable to intra-scan variability seen even between two scans of the same sequence. Here we examined performance of OSCILLATE in terms of consistency in recovered stiffness maps, which is the ultimate outcome of MRE, as opposed to consistency in reconstructed complex image series. The original image series includes physiological noise and other non-idealities, and as OSCILLATE seeks to primarily recover just the displacement information necessary for accurate stiffness estimation, comparison of image series can lead to inappropriate error metrics, while comparison of stiffness gives more appropriate and useful metrics.

Other acceleration techniques for MRE have focused on manipulating how the MEGs are applied to capture displacement in multiple directions over time. One concept for acquisition time reduction involves simultaneously applying each of the three motion encoding gradients. The Sample Interval Modulation (SLIM) MRE method proposes using

simultaneous motion encodings with the start time of each MEG shifted by a fraction of a period so that the accumulated phase in each direction can be differentiated using the temporal Fourier transform[24,25]. Nir et al proposed a similar method and applied three sinusoidal MEGs simultaneously uses varying start phases for each of the MEG sinusoid[26], while Guenthner et al used a Hadamard encoding technique to differentiate the accumulated phase[27]. Simultaneous directional encoding is an effective method for acquisition acceleration; however, they can be limited by the need for longer TE and the need to play individual gradients at a lower amplitude, impacting the SNR of recovered displacement fields. Each of these approaches can be beneficial depending on the application and base sequence, though it is unlikely that OSCILLATE could be effectively combined with either SLIM or Hadamard encoding, as the latter methods already acquire a reduced set of images and thus the low-rank subspace of OSCILLATE would provide less possibility for acceleration.

The OSCILLATE encoding and reconstruction scheme can be added to any multishot sequence, allowing the advantages of OSCILLATE to be used in addition to other advancements to acquisition speeds. We incorporated OSCILLATE into the 3D multiband, multishot MRE sequence and are able to retain all relevant components related to previous advances in data quality and speed, including the interleaved spiral shots for short readout time[69], the multiple k_z planes for multi-directional undersampling with SENSE parallel imaging, and motion-induced phase error correction. Similarly, OSCILLATE could be added to other novel MRE sequences, including the TURBINE-MRE sequence[22], in which multiple EPI readout blades are used to sample 3D *k*-space in a cylindrical pattern, or to the 3D spiral staircase sequence[21], which uses stack-of-spirals trajectory with each shot slightly varied in its k_z phase. The basic requirements of a sequence to add OSCILLATE are that the sequence must be multishot and the temporal basis must be able to be predetermined from a navigator image or alternate method. There are also many other ways to potentially exploit the low-rankness of MRE data in an image acquisition and reconstruction approach, including the incorporation of additional regularization terms, which may provide additional performance in improving speed or reducing error.

CONCLUSION

OSCILLATE is a method for accelerated magnetic resonance elastography which harnesses the highly spatiotemporally redundant nature of MRE data to allow for *k*-space undersampling through utilization of a joint low-rank image reconstruction. The OSCILLATE imaging and reconstruction pipeline is versatile and can be integrated with many existing MRE sequences. Here, we demonstrate the efficacy of the OSCILLATE method in a multiband MRE sequence where OSCILLATE allows for two-fold data undersampling, and a fifty percent reduction in acquisition times, with resulting stiffness maps having less than 1% global error. OSCILLATE potentially offers opportunities for even greater acceleration factors through combination with other advances such as compressed sensing and machine learning approaches. As brain MRE research shifts towards tailored sequences for specialized applications, fast acquisition scans that can maintain high resolution and low geometric distortion will become increasingly necessary. The OSCILLATE sequence allows for ease of scanning challenging populations such

as children or for inclusion of multiple MRE scans on a single subject under different conditions, and it may generally improve the adoptability of brain MRE in clinical protocols.

Supplementary Material

Refer to Web version on PubMed Central for supplementary material.

Acknowledgments

Support for this study was provided by the National Institutes of Health grants R01-EB027577, F31-HD103361, R01-AG058853, U01-NS112120, Delaware INBRE (P20-GM103446), and University of Delaware Research Foundation.

References

1. Manduca A, Oliphant TE, Dresner MA, et al. Magnetic resonance elastography: Non-invasive mapping of tissue elasticity. Med Image Anal. 2001;5(4):237–254. doi:10.1016/S1361-8415(00)00039-6 [PubMed: 11731304]
2. McIlvain G, Schwarb H, Cohen NJ, Telzer EH, Johnson CL. Mechanical properties of the in vivo adolescent human brain. Dev Cogn Neurosci. 2018;34:27–33. doi:10.1016/j.dcn.2018.06.001 [PubMed: 29906788]
3. Guo J, Bertalan G, Meierhofer D, et al. Brain maturation is associated with increasing tissue stiffness and decreasing tissue fluidity. Acta Biomater. 2019;99:433–442. doi:10.1016/j.actbio.2019.08.036 [PubMed: 31449927]
4. Sack I, Beierbach B, Wuerfel J, et al. The impact of aging and gender on brain viscoelasticity. Neuroimage. 2009;46(3):652–657. doi:10.1016/j.neuroimage.2009.02.040 [PubMed: 19281851]
5. Hiscox L, Johnson CL, McGarry MDJ, et al. High-resolution magnetic resonance elastography reveals differences in subcortical gray matter viscoelasticity between young and healthy older adults. Neurobiol Aging. 2018;65:158–167. doi:10.1016/j.neurobiolaging.2018.01.010 [PubMed: 29494862]
6. Murphy MC, Huston J III, Ehman RL, Huston J, Ehman RL. MR elastography of the brain and its application in neurological diseases. Neuroimage. 2019;187(August 2017):176–183. doi:10.1016/j.neuroimage.2017.10.008 [PubMed: 28993232]
7. Johnson CL, Schwarb H, Horecka KM, et al. Double dissociation of structure-function relationships in memory and fluid intelligence observed with magnetic resonance elastography. Neuroimage. 2018;171(December 2017):99–106. doi:10.1016/j.neuroimage.2018.01.007 [PubMed: 29317306]
8. Schwarb H, Johnson CL, Daugherty AM, et al. Aerobic fitness, hippocampal viscoelasticity, and relational memory performance. Neuroimage. 2017;153:179–188. doi:10.1016/j.neuroimage.2017.03.061 [PubMed: 28366763]
9. Johnson CL, Telzer EH. Magnetic resonance elastography for examining developmental changes in the mechanical properties of the brain. Dev Cogn Neurosci. 2018;33:176–181. doi:10.1016/j.dcn.2017.08.010 [PubMed: 29239832]
10. Delgorio PL, Hiscox LV, Daugherty AM, et al. Effect of Aging on the Viscoelastic Properties of Hippocampal Subfields Assessed with High-Resolution MR Elastography. Cereb Cortex. Published online 2021:1–13. doi:10.1093/cercor/bhaa388
11. Hiscox LV, McGarry MDJ, Johnson CL. Evaluation of cerebral cortex viscoelastic property estimation with nonlinear inversion magnetic resonance elastography. Phys Med Biol. Published online 2022.
12. Schmidt JL, Tweten DJ, Badachhape AA, et al. Measurement of anisotropic mechanical properties in porcine brain white matter ex vivo using magnetic resonance elastography. J Mech Behav Biomed Mater. 2017;79(December 2017):30–37. doi:10.1016/j.jmbbm.2017.11.045 [PubMed: 29253729]

13. Babaei B, Fovargue D, Lloyd RA, et al. Magnetic Resonance Elastography Reconstruction for Anisotropic Tissues. Med Image Anal. Published online 2021:In Press. doi:10.1016/j.media.2021.102212
14. Smith DR, Guertler CA, Okamoto RJ, Romano AJ, Bayly PV, Johnson CL. Multi-excitation magnetic resonance elastography of the brain: Wave propagation in anisotropic white matter. J Biomech Eng. 2020;142(7). doi:10.1115/1.4046199
15. Anderson AT, Van Houten EEW, McGarry MDJ, et al. Observation of direction-dependent mechanical properties in the human brain with multi-excitation MR elastography. J Mech Behav Biomed Mater. 2016;59:538–546. doi:10.1016/j.jmbbm.2016.03.005 [PubMed: 27032311]
16. Posnansky O, Guo J, Hirsch S, Papazoglou S, Braun J, Sack I. Fractal network dimension and viscoelastic powerlaw behavior: I. A modeling approach based on a coarse-graining procedure combined with shear oscillatory rheometry. Phys Med Biol. 2012;57(12):4023–4040. doi:10.1088/0031-9155/57/12/4023 [PubMed: 22674184]
17. Guo J, Posnansky O, Hirsch S, Scheel M. Fractal network dimension and viscoelastic powerlaw behavior : II. An experimental study of structure-mimicking phantoms by magnetic resonance elastography Fractal network dimension and viscoelastic powerlaw behavior : II. An experimental study of struc. Phys Med Biol. Published online 2012. doi:10.1088/0031-9155/57/12/4041
18. Murphy MC, Glaser KJ, Manduca A, Felmlee JP, Huston J, Ehman RL. Analysis of time reduction methods for magnetic resonance elastography of the brain. Magn Reson Imaging. 2010;28(10):1514–1524. [PubMed: 20817440]
19. Ebersole C, Ahmad R, Rich AV., Potter LC, Dong H, Kolipaka A. A bayesian method for accelerated magnetic resonance elastography of the liver. Magn Reson Med. 2018;80(3):1178–1188. doi:10.1002/mrm.27083 [PubMed: 29334131]
20. Johnson CL, Holtrop JL, McGarry MDJ, et al. 3D multislab, multishot acquisition for fast, whole-brain MR elastography with high signal-to-noise efficiency. Magn Reson Med. 2014;71(2):477–485. doi:10.1002/mrm.25065 [PubMed: 24347237]
21. Peng X, Sui Y, Trzasko JD, et al. Fast 3D MR elastography of the whole brain using spiral staircase: Data acquisition, image reconstruction, and joint deblurring. Magn Reson Med. 2021;(August 2020):1–14. doi:10.1002/mrm.28855
22. Sui Y, Arani A, Trzasko JD, et al. TURBINE-MRE: A 3D Hybrid Radial-Cartesian EPI Acquisition for MR Elastography Yi. Magn Reson Med. 2021;85(2):945–952. doi:10.1002/mrm.28445.TURBINE-MRE [PubMed: 32738084]
23. Braun J, Guo J, Lützkendorf R, et al. High-resolution mechanical imaging of the human brain by three-dimensional multifrequency magnetic resonance elastography at 7T. Neuroimage. 2014;90:308–314. doi:10.1016/j.neuroimage.2013.12.032 [PubMed: 24368262]
24. Klatt D, Yasar TK, Royston TJ, Magin RL. Sample interval modulation for the simultaneous acquisition of displacement vector data in magnetic resonance elastography: Theory and application. Phys Med Biol. 2013;58(24):8663–8675. doi:10.1088/0031-9155/58/24/8663 [PubMed: 24256743]
25. Klatt D, Johnson CL, Magin RL. Simultaneous, Multidirectional Acquisition of Displacement Fields in Magnetic Resonance Elastography of the In Vivo Human Brain. J Magn Reson Imaging. 2015;42(2):297–304. doi:10.1002/jmri.24806 [PubMed: 25425147]
26. Nir G, Sahebjavaher RS, Sinkus R, Salcudean SE. A framework for optimization-based design of motion encoding in magnetic resonance elastography. Magn Reson Med. 2015;73(4):1514–1525. doi:10.1002/mrm.25280 [PubMed: 24803300]
27. Guenthner C, Runge JH, Sinkus R, Kozerke S. Analysis and improvement of motion encoding in magnetic resonance elastography. NMR Biomed. 2018;31(5):1–18. doi:10.1002/nbm.3908
28. Garteiser P, Sahebjavaher RS, Ter Beek LC, et al. Rapid acquisition of multifrequency, multislice and multidirectional MR elastography data with a fractionally encoded gradient echo sequence. NMR Biomed. 2013;26(10):1326–1335. doi:10.1002/nbm.2958 [PubMed: 23712852]
29. Guenthner C, Sethi S, Troelstra M, Dokumaci AS, Sinkus R, Kozerke S. Ristretto MRE: A generalized multi-shot GRE-MRE sequence. NMR Biomed. 2019;32(5):1–13. doi:10.1002/nbm.4049

30. Otazo R, Candès E, Sodickson DK. Low-rank plus sparse matrix decomposition for accelerated dynamic MRI with separation of background and dynamic components. Magn Reson Med. 2015;73(3):1125–1136. doi:10.1002/mrm.25240 [PubMed: 24760724]
31. Haldar JP. Low-Rank Modeling of Local k-Space Neighborhoods (LORAKS) for Constrained MRI. IEEE Trans Med Imaging. 2014;33(3):668–681. doi:10.1109/TMI.2013.2293974 [PubMed: 24595341]
32. Zhao B, Lu W, Hitchens TK, Lam F, Ho C, Liang ZP. Accelerated MR parameter mapping with low-rank and sparsity constraints. Magn Reson Med. 2015;74(2):489–498. doi:10.1002/mrm.25421 [PubMed: 25163720]
33. Lam F, Ma C, Clifford B, Johnson CL, Liang ZP. High-resolution 1H-MRSI of the brain using SPICE: Data acquisition and image reconstruction. Magn Reson Med. 2016;76(4):1059–1070. doi:10.1002/mrm.26019 [PubMed: 26509928]
34. Meng Z, Guo R, Li Y, et al. Accelerating T2 mapping of the brain by integrating deep learning priors with low-rank and sparse modeling. Magn Reson Med. 2021;85(3):1455–1467. doi:10.1002/mrm.28526 [PubMed: 32989816]
35. Mani M, Jacob M, Kelley D, Magnotta V. Multi-shot sensitivity-encoded diffusion data recovery using structured low-rank matrix completion (MUSSELS). Magn Reson Med. 2017;78(2):494–507. doi:10.1002/mrm.26382 [PubMed: 27550212]
36. Chiew M, Graedel NN, Miller KL. Recovering task fMRI signals from highly under-sampled data with low-rank and temporal subspace constraints. Neuroimage. 2018;174(February):97–110. doi:10.1016/j.neuroimage.2018.02.062 [PubMed: 29501875]
37. Mason HT, Graedel NN, Miller KL, Chiew M. Subspace-constrained approaches to low-rank fMRI acceleration. Neuroimage. 2021;238(December 2020):118235. doi:10.1016/j.neuroimage.2021.118235 [PubMed: 34091032]
38. Guo S, Fessler JA, Noll DC. High-Resolution Oscillating Steady-State fMRI. IEEE Trans Med Imaging. 2020;39(12):4357–4368. [PubMed: 32809938]
39. Christodoulou AG, Zhang H, Zhao B, Hitchens TK, Ho C, Liang ZP. High-resolution cardiovascular MRI by integrating parallel imaging with low-rankand sparse modeling. IEEE Trans Biomed Eng. 2013;60(11):3083–3092. doi:10.1109/TBME.2013.2266096 [PubMed: 23744657]
40. Zhao B, Haldar JP, Brinegar C, Liang ZP. Low rank matrix recovery for real-time cardiac MRI. 2010 7th IEEE Int Symp Biomed Imaging From Nano to Macro, ISBI 2010 - Proc. 2010;(4):996–999. doi:10.1109/ISBI.2010.5490156
41. Tremoulheac B, Dikaios N, Atkinson D, Arridge SR. Dynamic MR image reconstruction-separation from undersampled (k,t)-Space via low-rank plus sparse prior. IEEE Trans Med Imaging. 2014;33(8):1689–1701. doi:10.1109/TMI.2014.2321190 [PubMed: 24802294]
42. McIlvain G, Cerjanic AM, Christodoulou AG, McGarry MD, Johnson CL. OSCILLATE: A Low-Rank Approach for Accelerated Magnetic Resonance Elastography. In: 28th Annual Meeting of the International Society for Magnetic Resonance in Medicine.; 2020.
43. Liang Z Spatiotemporal Imagingwith Partially Separable Functions. 2007 4th IEEE Int Symp Biomed Imaging From Nano to Macro. 2007;2:988–991. doi:10.1109/ISBI.2007.357020
44. Hannum AJ, McIlvain G, Sowinski D, McGarry MDJ, Johnson CL. Correlated Noise in Brain Magnetic Resonance Elastography. Magn Reson Med. Published online 2021. doi:10.1002/mrm.29050
45. Johnson CL, Holtrop JL, Anderson AT, Sutton BP. Brain MR Elastography with Multiband Excitation and Nonlinear Motion-Induced Phase Error Correction. In: 24th Annual Meeting of the Interational Society for Magnetic Resonance in Medicine, Singapore.; 2016:p 1951.
46. Glover GH. Simple Analytic Spiral K-Space Algorithm. Magn Reson Med. 1999;415:412–415.
47. Pruessmann KP, Weiger M, Bornert P, Boesiger P. Advances in sensitivity encoding with arbitrary k-space trajectories. Magn Reson Med. 2001;461(4):638–651.
48. Johnson CL, McGarry MDJ, Van Houten EEW, et al. Magnetic resonance elastography of the brain using multishot spiral readouts with self-navigated motion correction. Magn Reson Med. 2013;70(2):404–412. doi:10.1002/mrm.24473 [PubMed: 23001771]

49. Zahneisen B, Poser BA, Ernst T, Stenger VA. Three-dimensional Fourier encoding of simultaneously excited slices: Generalized acquisition and reconstruction framework. Magn Reson Med. 2014;71(6):2071–2081. doi:10.1002/mrm.24875 [PubMed: 23878075]
50. Liu C, Bammer R, Kim DH, Moseley ME. Self-navigated interleaved spiral (SNAILS): Application to high-resolution diffusion tensor imaging. Magn Reson Med. 2004;52(6):1388–1396. doi:10.1002/mrm.20288 [PubMed: 15562493]
51. Sutton BP, Noll DC, Fessler JA. Fast, Iterative Image Reconstruction for MRI in the Presence of Field Inhomogeneities. IEEE Trans Med Imaging. 2003;22(2):178–188. [PubMed: 12715994]
52. Funai AK, Fessler JA, Yeo DTB, Noll DC, Olafsson VT. Regularized field map estimation in MRI. IEEE Trans Med Imaging. 2008;27(10):1484–1494. doi:10.1109/TMI.2008.923956 [PubMed: 18815100]
53. Cerjanic A, Holtrop JL, Ngo GC, et al. PowerGrid: A open source library for accelerated iterative magnetic resonance image reconstruction. Proc Intl Soc Mag Reson Med. Published online 2016:14–17.
54. McGarry MDJ, Van Houten EEW, Johnson CL, et al. Multiresolution MR elastography using nonlinear inversion. Med Phys. 2012;39(10):6388–6396. doi:10.1118/1.4754649 [PubMed: 23039674]
55. Van Houten EEW, Miga MI, Weaver JB, Kennedy FE, Paulsen KD. Three-dimensional subzoned-based reconstruction algorithm for MR elastography. Magn Reson Med. 2001;45:827–837. doi:10.1002/mrm.1111 [PubMed: 11323809]
56. Zhang Y, Brady M, Smith S. Segmentation of brain MR images through a hidden Markov random field model and the expectation-maximization algorithm. IEEE Trans Med Imaging. 2001;20(1):45–57. doi:10.1109/42.906424 [PubMed: 11293691]
57. Jenkinson M, Smith S. A global optimisation method for robust affine registration of brain images. Med Image Anal. 2001;5(2):143–156. doi:10.1016/S1361-8415(01)00036-6 [PubMed: 11516708]
58. Jenkinson M, Beckmann CF, Behrens TEJJ, Woolrich MW, Smith SM. Fsl. Neuroimage. 2012;62(2):782–790. doi:10.1016/j.neuroimage.2011.09.015 [PubMed: 21979382]
59. Kim DH, Adalsteinsson E, Spielman DM. Simple analytic variable density spiral design. Magn Reson Med. 2003;50(1):214–219. doi:10.1002/mrm.10493 [PubMed: 12815699]
60. Gallichan D, Andersson JLR, Jenkinson M, Robson MD, Miller KL. Reducing distortions in diffusion-weighted echo planar imaging with a dual-echo blip-reversed sequence. Magn Reson Med. 2010;64(2):382–390. doi:10.1002/mrm.22318 [PubMed: 20665782]
61. Sack I, Beierbach B, Hamhaber U, Klatt D. Non-invasive measurement of brain viscoelasticity using magnetic resonance elastography. NMR Biomed. 2008;21(July 2007):265–271. doi:10.1002/nbm [PubMed: 17614101]
62. Johnson CL, Schwarb H, McGarry MDJ, et al. Viscoelasticity of subcortical gray matter structures. Hum Brain Mapp. 2016;37:4221–4233. doi:10.1002/hbm.23314 [PubMed: 27401228]
63. Murphy MC, Huston J, Jack CR, et al. Measuring the characteristic topography of brain stiffness with magnetic resonance elastography. PLoS One. Published online 2013. doi:10.1371/journal.pone.0081668
64. Okamoto RJ, Clayton EH, Bayly PV. Viscoelastic properties of soft gels: Comparison of magnetic resonance elastography and dynamic shear testing in the shear wave regime. Phys Med Biol. 2011;56(19):6379–6400. doi:10.1088/0031-9155/56/19/014 [PubMed: 21908903]
65. Papazoglou S, Hirsch S, Braun J, Sack I. Multifrequency inversion in magnetic resonance elastography. Phys Med Biol. 2012;57(8):2329–2346. doi:10.1088/0031-9155/57/8/2329 [PubMed: 22460134]
66. Oliphant TE, Manduca A, Ehman RL, Greenleaf JF. Complex-valued stiffness reconstruction for magnetic resonance elastography by algebraic inversion of the differential equation. Magn Reson Med. 2001;45(2):299–310. doi:10.1002/1522-2594(200102)45:2<299::AID-MRM1039>3.0.CO;2-O [PubMed: 11180438]
67. Murphy MC, Manduca A, Trzasko JD, Glaser KJ, Huston J, Ehman RL. Artificial neural networks for stiffness estimation in magnetic resonance elastography. Magn Reson Med. 2018;80(1):351–360. doi:10.1002/mrm.27019 [PubMed: 29193306]

68. Scott JM, Arani A, Manduca A, et al. Artificial Neural Networks for Magnetic Resonance Elastography Stiffness Estimation in Inhomogeneous Materials. Med Image Anal. 2020;63:101710. doi:10.1016/j.media.2020.101710.Artificial [PubMed: 32442867]

69. McIlvain G, McGarry MDJ, Johnson CL. Quantitative Effects of Off-Resonance Related Distortion on Brain Mechanical Property Estimation with Magnetic Resonance Elastography. NMR Biomed. Published online 2021:In Press.

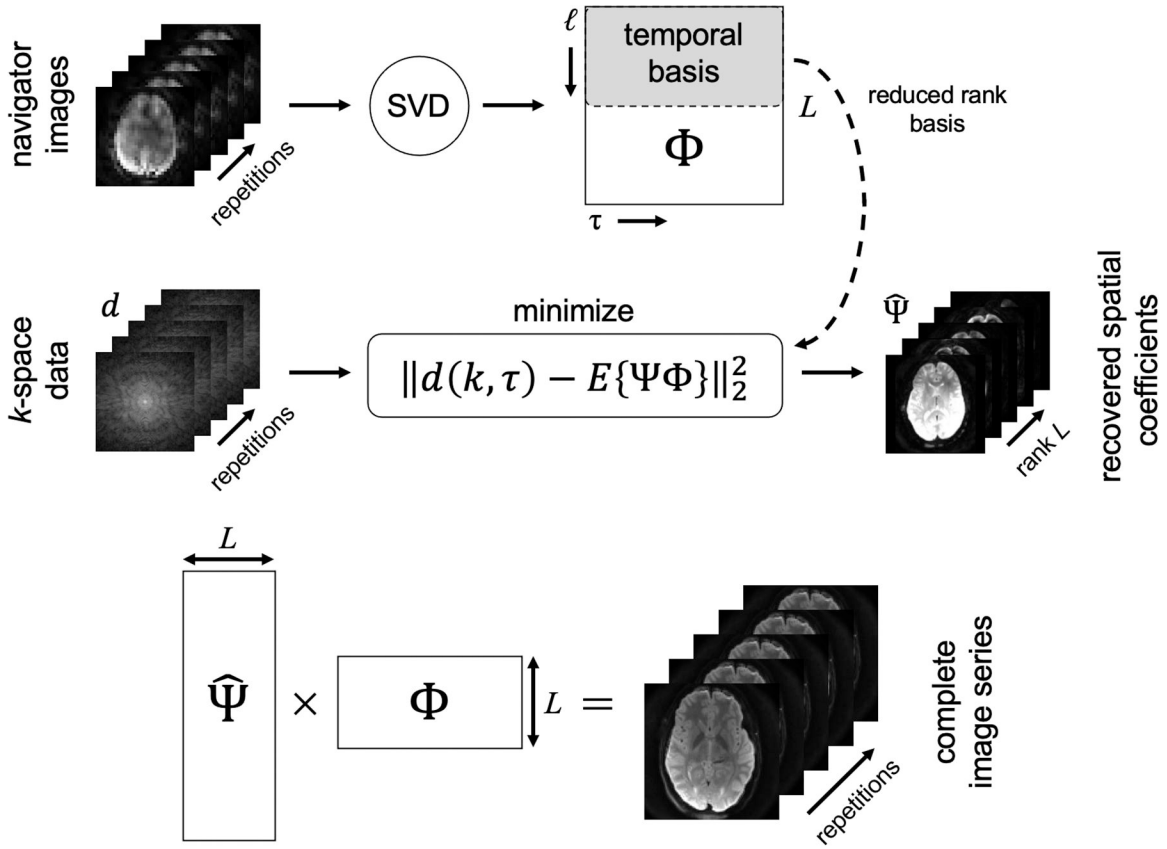

Figure 1:

OSCILLATE image reconstruction. Navigator images are decomposed to find the temporal basis Φ, which is then truncated to a reduced rank. The objective function is used to determine the spatial coefficients by minimizing the difference between undersampled k-space data and known Φ. Recovered spatial coefficients and known temporal basis are combined to recover the entire complex image series.

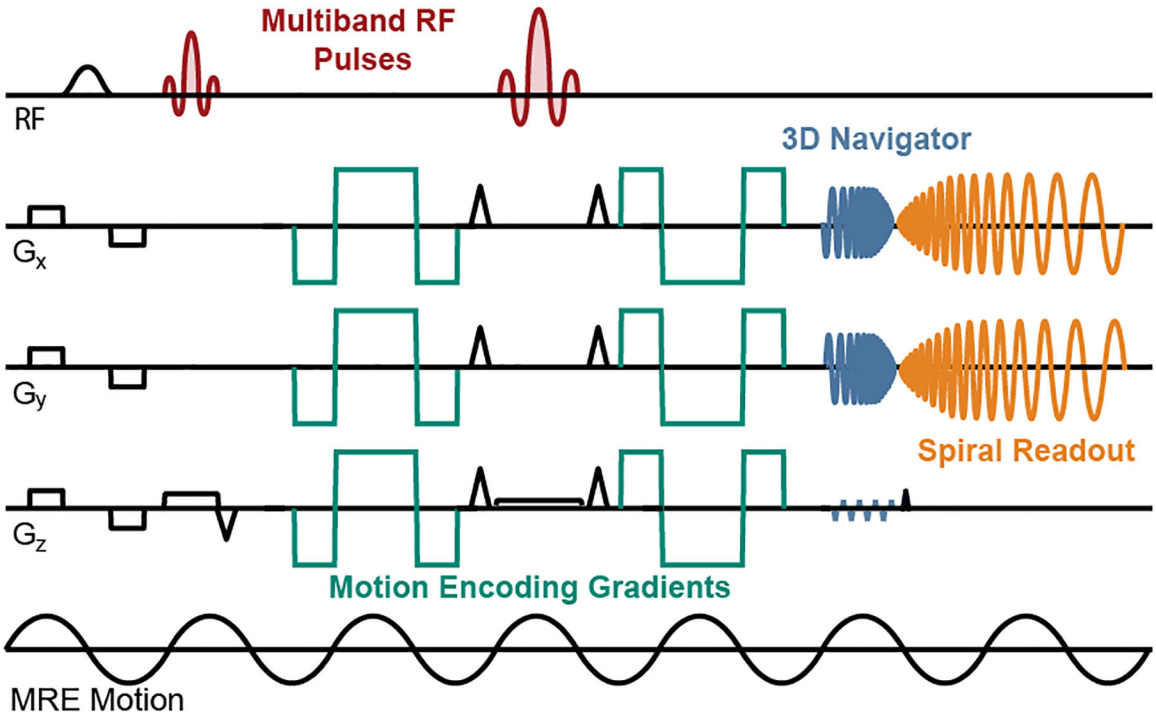

Figure 2:

3D multiband, multishot spiral, spin-echo MRE sequence diagram for OSCILLATE implementation. The sequence comprises 90° excitation and 180° refocusing multiband RF pulses; bilateral, flow compensated, motion encoding gradients, which are applied on one axis at a time; k_z-blipped spiral-in 3D navigator, which is used for motion-induced phase error correction and estimation of temporal basis functions; and a multishot k_{xy} spiral out image readout. OSCILLATE is implemented by alternating which spiral shots are sampled across repetitions.

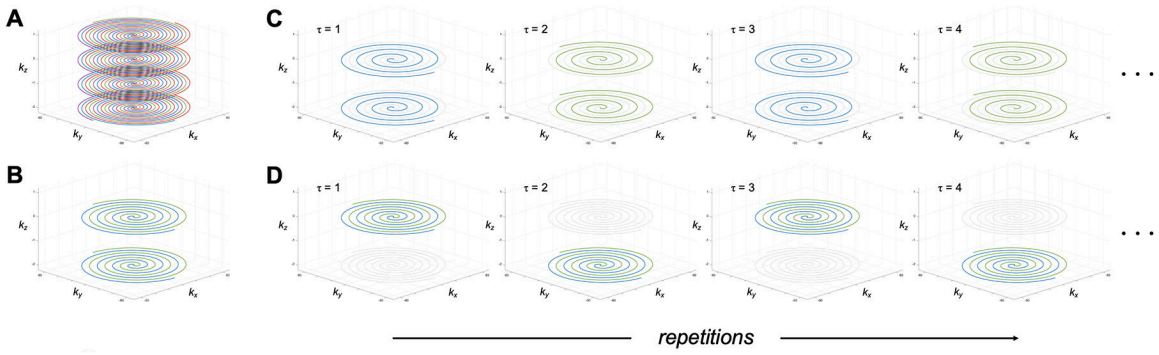

Figure 3:

3D multiband, mutlishot, spiral k-space sample patterns for A) fully sampled k-space B) undersampled k-space from SENSE parallel imaging at $R_{SENSE} = 4$, C) undersampled k-space from OSCILLATE at $R_{OSC} = 2$ with k_{xy} shots undersampled and D) undersampled k-space from OSCILLATE at $R_{OSC} = 2$ with k_z planes undersampled.

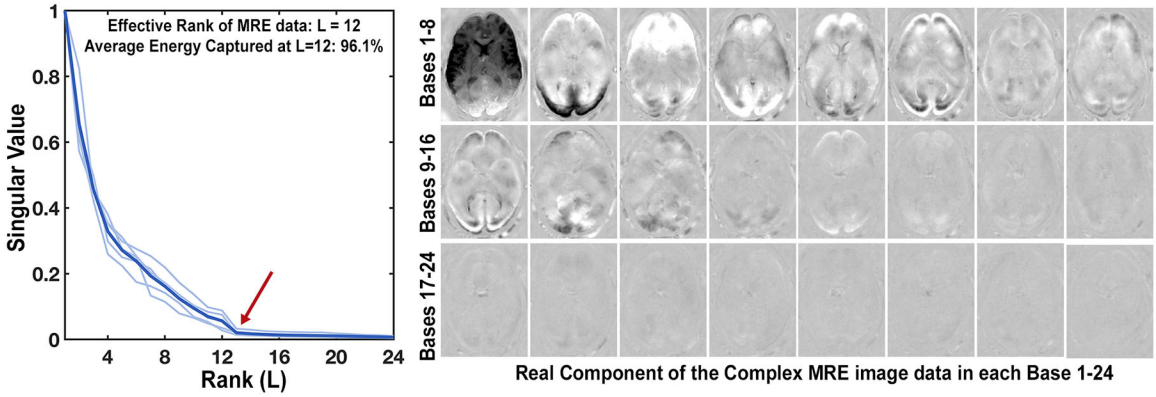

Figure 4:

MRE data is accurately recoverable at reduced rank of 12 from its full rank of 24. Singular value decomposition shows that nearly all MRE data energy is captured at or below L=12 (sum of bases 1–12 = 96.1%).

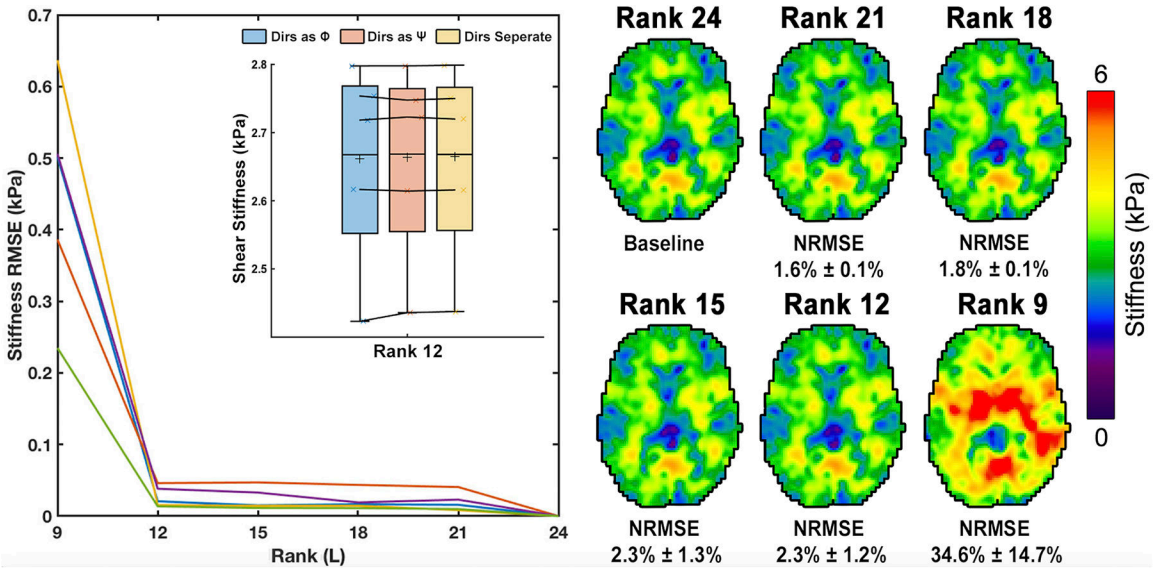

Figure 5:

Results from truncating complex MRE image data and inverting displacement fields from reduced rank images into maps of stiffness. Plot shows RMSE for the five subjects at each reduced rank truncation, with insert showing the results from the methods of forming the Casorati matrix for decomposing the dataset: encoding directions as ‘time’, Φ, or as ‘space’, Ψ, or separately. Corresponding stiffness map images from a single representative subject with NRMSE from reference rank 24 averaged across the five subjects.

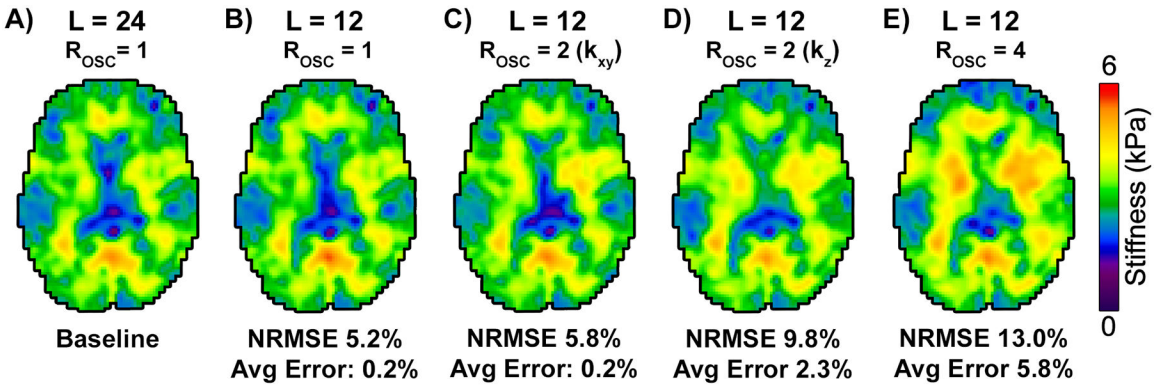

Figure 6:

Retrospective OSCILLATE reconstruction of fully-sampled (R_{OSC} = 1) k-space data at A) full rank (L = 24) and B) reduced rank (L = 12), and undersampled k-space data in different sampling patterns, including: C) R_{OSC} =2, k_{xy} shots; D) R_{OSC} =2, k_z planes; and E) R_{OSC} =4, both k_{xy} and k_z.

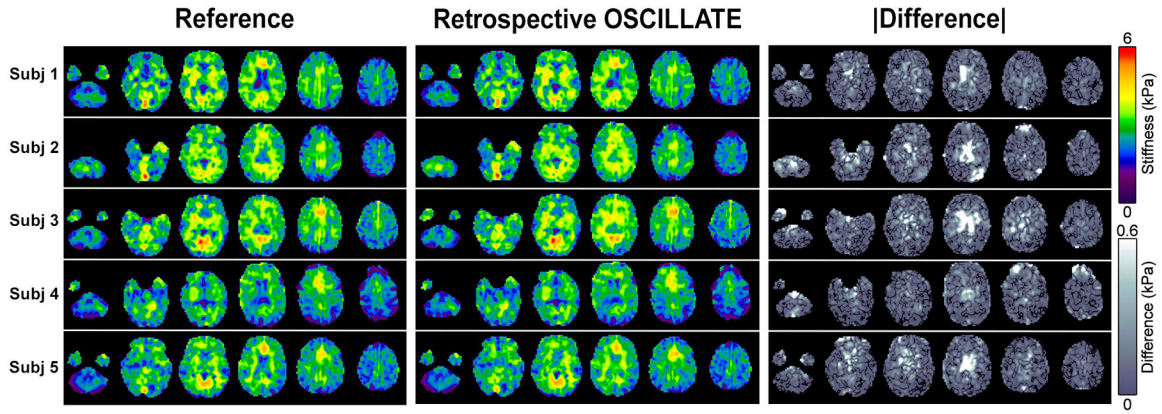

Figure 7:

Stiffness maps from retrospectively undersampled data reconstructed with OSCILLATE at $R_{OSC} = 2$, as well as reference data for each of the five subjects. Absolute difference maps show errors are concentrated in the ventricle regions with estimates of brain tissue stiffness having only small and distributed errors. Absolute difference maps are scaled 10x relative to stiffness maps to allow for visualization.

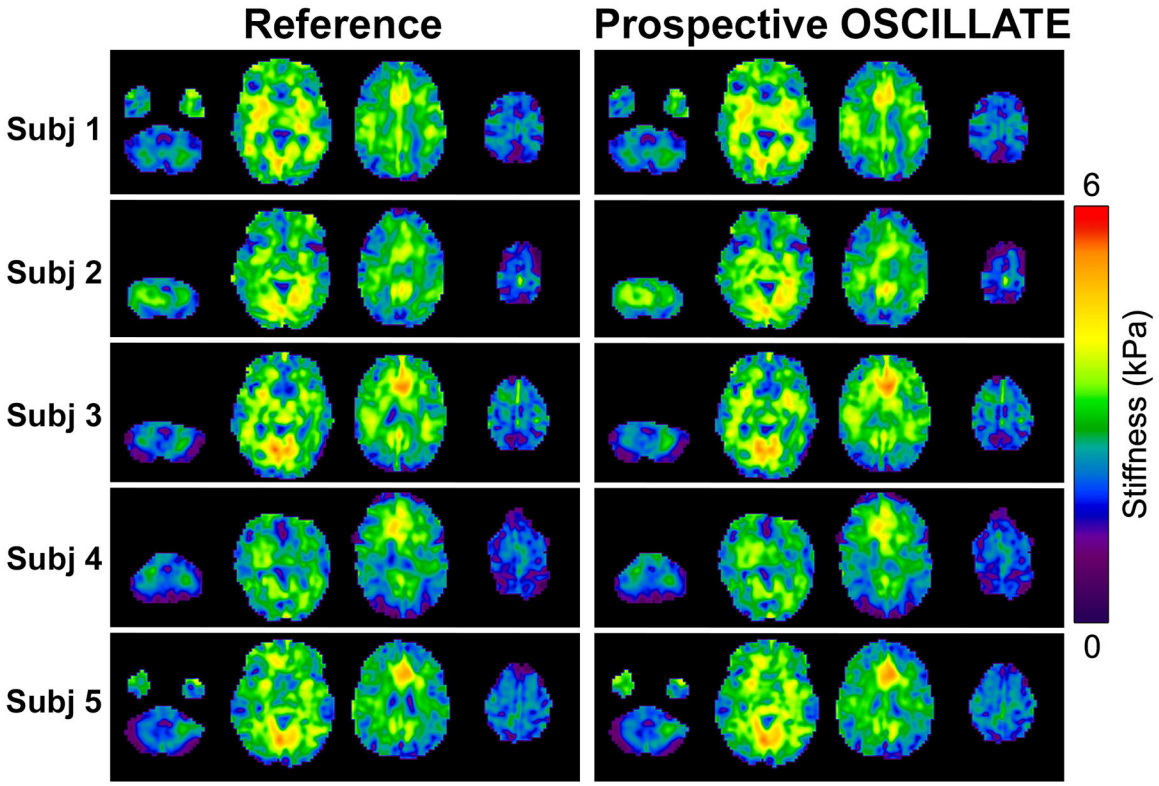

Figure 8:

Stiffness maps from prospectively undersampled OSCILLATE data at R_{OSC} =2 compared with stiffness maps from the original multiband MRE sequence as reference for each of the five subjects. The OSCILLATE scan took 1 minute 48 seconds, and global stiffness errors between the OSCILLATE scan and the fully sampled MBMRE scan was 1.0% ± 0.7% across the five subjects.